Published in final edited form as:

Clin Cancer Res. 2015 October 15; 21(20): 4576–4585. doi:10.1158/1078-0432.CCR-15-0314.

Targeting Acidity in Pancreatic Adenocarcinoma: Multispectral Optoacoustic Tomography Detects pH-low Insertion Peptide Probes *in vivo*

Charles W Kimbrough, MD[1], **Anil Khanal, PhD**[2], **Matthew Zeiderman, BS**[1], **Bigya R. Khanal, MS**[2], **Neal C Burton, PhD**[3], **Kelly M McMasters, MD/PhD**[1], **Selwyn Vickers, MD**[4], **William E Grizzle, MD/PhD**[4], and **Lacey R McNally, PhD**[2]

[1]The Hiram C. Polk Jr., MD Department of Surgery, University of Louisville, Louisville, KY

[2]Department of Medicine, University of Louisville, Louisville, KY

[3]iThera Medical, Munich, Germany

[4]University of Alabama at Birmingham, Birmingham, AL

Abstract

Background—pH-low Insertion Peptides (pHLIPs) can serve as a targeting moiety that enables pH-sensitive probes to detect solid tumors. Using these probes in conjunction with multispectral optoacoustic tomography (MSOT) is a promising approach to improve imaging for pancreatic cancer.

Methods—A pH-sensitive pHLIP (V7) was conjugated to 750 NIR fluorescent dye and evaluated as a targeted probe for pancreatic adenocarcinoma. The pH-insensitive K7 pHLIP served as an untargeted control. Probe binding was assessed *in vitro* at pH 7.4, 6.8, and 6.6 using human pancreatic cell lines S2VP10 and S2013. Using MSOT, semi-quantitative probe accumulation was then assessed *in vivo* with a murine orthotopic pancreatic adenocarcinoma model.

Results—*In vitro*, the V7–750 probe demonstrated significantly higher fluorescence at pH 6.6 compared to pH 7.4 (S2VP10, p=0.0119; S2013, p=0.0160), while no difference was observed with the K7–750 control (S2VP10, p=0.8783; S2013, p=0.921). In the *in vivo* S2VP10 model, V7–750 probe resulted in 782.5 MSOT a.u. signal compared to 5.3 MSOT a.u. in K7–750 control in tumor (p= 0.0001). Similarly, V7–750 probe signal was 578.3 MSOT a.u. in the S2013 model compared to K7–750 signal at 5.1 MSOT a.u. (p=0.0005). There was minimal off-target accumulation of the V7–750 probe within the liver or kidney, and probe distribution was confirmed with *ex vivo* imaging.

Conclusion—Compared to pH-insensitive controls, V7–750 pH-sensitive probe specifically targets pancreatic adenocarcinoma, and has minimal off-target accumulation. The non-invasive detection of pH-targeted probes by means of MSOT represents a promising modality to improve the detection and monitoring of pancreatic cancer.

Corresponding Author: Lacey R. McNally, Department of Medicine, University of Louisville School of Medicine, Louisville, KY 40202, ph 502-852-2288, lrmcna01@louisville.edu.

Introduction

Since the 1970s, there has been little change in the outcomes of patients with pancreatic ductal adenocarcinoma (PDAC), and the overall 5-year survival remains approximately 5%. (1) Despite this persistent poor overall survival, over the last decade advances in imaging technology have greatly impacted management in PDAC patients. Imaging modalities including ultrasound (US), endoscopic ultrasound (EUS), CT, MRI, and PET currently all have a central role in the clinical management of pancreatic cancer. The role of imaging extends to all aspects of care, including the diagnosis and characterization of pancreatic masses, patient follow-up and monitoring, and screening high-risk patients. (2) For instance, pre-operative imaging is essential to help determine resectability, particularly in patients with borderline tumors. In addition, with the use of fluorescent probes, there may be an emerging role for intraoperative margin assessment during the resection of solid tumors. (3) Because complete surgical resection of PDAC in patients with early localized disease may increase 5-year survival rates up to 30–60%, imaging modalities that identify patients earlier in the disease process, improve the characterization of tumors, or help ensure margin-negative resections have the potential to increase survival in patients with pancreatic cancer. (2)

Optoacoustic (photoacoustic) imaging is an emerging new technology with the potential to increase sensitivity and improve 3D spatial resolution in the imaging of solid tumors. Through the use of non-ionizing electromagnetic waves that subsequently induce a detectable acoustic signal, optoacoustic imaging represents a hybrid technique that incorporates advantageous properties of both light and sound. (4) Optoacoustic imaging is currently unique in that the resolution of the optical contrast obeys the rules of ultrasonic diffraction, rendering photon scattering irrelevant to image resolution. Thus, it yields high-resolution at depth to provide insights into the biological function of entire tumors and organs. (5) Although multispectral optoacoustic tomography (MSOT) has the potential to increase both image resolution and sensitivity, the development of specific molecular probes to serve as optical contrast agents is critical to leverage the capabilities of this technology for cancer detection in living subjects. (6)

In general, these exogenous contrast agents work in one of two ways. They can be non-targeted, and rely on the enhanced permeability and retention effect in order to concentrate within tumors, or they can be designed to specifically target tumor cells. Tumor-specific probes are typically constructed by conjugating a fluorophore to a specific ligand that targets cell surface proteins upregulated on tumor cells. (7–10) These cell surface proteins are typically some type of specific molecular receptor such as epidermal growth factor receptor (EGFr). (9–10) Unfortunately, these surface receptors are frequently heterogeneously expressed among different patients, and will even vary among the clonal populations that comprise a single tumor. (11) Tumors are complex environments, where altered cellular signaling, genetic and epigenetic deregulations, and interactions with the microenvironment contribute to a constantly changing phenotype, including the expression of extracellular proteins. (12) Furthermore, although these extracellular receptors are over expressed on tumor cells, they are not tumor-specific, and are often found on non-malignant tissue such as the liver or kidney. Because sub-populations of malignant cells within the same tumor may

phenotypically express different numbers and types of receptors, the use of any single surface protein as a target for molecular imaging might result in inadequate or inconsistent tumor detection. (13)

To overcome the limitations inherent in targeting heterogeneous cell surface proteins, novel imaging technologies have been developed that focus on the acidic microenvironment of cancer cells. (14–15) Ischemia and acidosis frequently accompany tumor progression from early to advanced stages, related to factors such as hypoxia, the Warburg effect, and carbonic anhydrases. (16) Therefore, compared to specific molecular markers, tumor acidity may provide a more universal target for imaging and therapy. (17–19) Moreover, as a major component of the tumor microenvironment, low tumor pH may play an important role in tumor progression by regulating angiogenesis and chemoresistance by protonating chemotherapeutics. (18, 20) Our hypothesis is that targeting the acidic extracellular pH (pH_e) of pancreatic tumors can circumvent the problems associated with the targeting of heterogeneous surface proteins. To target acidic extracellular pH, we will utilize the novel technology of pH low insertion peptides (pHLIPs), which reversibly fold and insert across membranes in response to pH changes (Figure 1). (21, 22)

In this study, we utilized the V7 pHLIP to create a pH-sensitive probe (V7–750) in order to help identify pancreatic tumors with MSOT. The modified pH-insensitive K7 pHLIP with a single Glu to Lys substitution in the carboxy-terminal end was used to make a pH-insensitive control. (21) Through MSOT, we were able to assess probe localization volumetrically (i.e., in 3D), as well as to separate the probe signal from adjacent uninvolved tissues and organs. Our results provide evidence that pH-sensitive probes facilitate detection of pancreatic cancer by MSOT *in vivo*. The translation of this imaging modality to pancreatic cancer is promising due to the recent development and early testing of MSOT equipment for clinical use. (23–25)

Methods

1) Cell Culture and reagents

The human pancreatic cancer cell lines S2VP10 and S2013 were kindly provided by M. Hollingsworth (University of Nebraska). Luciferase clones of these pancreatic cells were previously described. (9, 10) Cell culture media was constructed by mixing RPMI-1640 powder in a phosphate buffer solution prepared at either pH 7.4, 6.8, or 6.6. The pH-specific phosphate buffers (25 mM) were prepared by mixing sodium phosphate monobasic and sodium phosphate dibasic (Sigma-Aldrich, St. Louis, USA) in distilled water; sodium bicarbonate was not added in order to prevent the induction of carbonic acid. Afterwards, the phosphate buffers were sterilized by autoclaving. To create the pH-specific media, 13.6 gm of RPMI media 1640 powder (Life Technologies, Grand Island, NY, USA) was dissolved into each solution of pH-specific phosphate buffer (1L, 25 mM). Afterwards, the RPMI media solutions were filtered through sterilized What man qualitative filter paper, grade-1 (Sigma-Aldrich, St. Louis, USA) and then mixed with 10% fetal bovine serum (Atlanta Biologicals, Lawrenceville, GA, USA) and 1% L-glutamine (Life Technologies, Grand Island, NY, USA). The final pH of each supplemented RPMI solution was checked by pH meter (Denver Instrument Ultrabasic, Bohemia, NY, USA), and if required, pH was

maintained by adding sterilized sodium hydroxide (1M) or hydrochloric acid (1M). Cells were grown in supplemented RPMI media (pH 7.4) and incubated at 37° C in the absence of CO_2.

2) Labelling pHLIPS with NIR dye

The V7 pHLIP amino acid sequence, with the transmembrane portion underlined, is Ala-Cys-Glu-Glu-Gln-Asn-Pro-Trp-Ala-Arg-Tyr-Leu-Glu-Trp-Leu-Phe-Pro-Thr-Glu-Thr-Leu-Leu-Leu-Glu-Leu. The sequence for the pH insensitive K7 pHLIP is Ala-Cys-Glu-Glu-Gln-Asn-Pro-Trp-Ala-Arg-Tyr-Leu-Glu-Trp-Leu-Phe-Pro-Thr-Glu-Thr-Leu-Leu-Leu-Lys-Leu. Both the V7 and K7 probes were synthesized at CS Bio (Menlo Park, CA, USA). The amino acid sequences for V7 and K7 are the same except for a Lys residue substitution for Glu in K7 at the 24th amino acid.

HiLyte Fluor™ 750 C2 maleimide (AnaSpec, Fremont, CA) was conjugated with Cys residues placed on the N-terminus group in the V7 or K7 peptides to create the pH-sensitive (V7–750) and pH-insensitive probes (K7–750) as described by supplier's protocol. V7 or K7 peptide (0.0007 gm) was dissolved in 0.3 mL phosphate buffer (25 mM, pH 7.4) and mixed with 110 μL of HiLyte Fluor™ 750 C2 maleimide (2.7 mM) in N,N-Dimethylformamide (Sigma-Aldrich, St. Louis, USA) overnight at room temperature. Then, the V7–750 or K7–750 probe was transferred into dialysis tubing (2000 nominal molecular weight cut-off (NMWCO), Sigma-Aldrich, St. Louis, USA) and dialyzed against phosphate buffer (25 mM, 0.5 % NaCl, pH 7.4) to remove the excess of free dye. Dialysis was performed for one day by exchanging phosphate buffer at 4-hour time intervals for a total of 5 exchanges. The stock solution of V7–750 or K7–750 (652 uM) in phosphate buffer (25 mM, 0.5 % NaCl, pH 7.4) was diluted further to obtain the desired concentration prior to any planned experiment. The conjugation of HiLyte Fluor™ 750 C2 maleimide with V7–750 or K7–750 was confirmed by a UV-Visible (UV-Vis) spectrophotometer (Cary 100, Varian, CA, USA). UV-Vis spectrophotometry showed absorbance maxima at 280 and 750 nm (due to the peptide and dye, respectively), and both probes showed almost the same absorbance spectrum (Supplemental Figure S1A).

3) In vitro analysis of pHLIP binding at pH

The human pancreatic cell lines S2VP10 and S2013 were plated in 6-well plates at 5.0×10^5 cells per well using RPMI media (pH 7.4) supplemented with 1% glutamine and 10% fetal bovine serum. Once cells had attached to the plates, the RPMI media was removed and the cells were washed with phosphate buffer (25 mM, pH 7.4). Afterwards, pH-specific RPMI media of pH 7.4, 6.8, or 6.6 was added to the wells and cells were incubated overnight at 37°C without CO_2. The pH of the wells was confirmed using a needle-tip pH electrode (ORION® needle-tip micro combination pH electrode, Thermo scientific, PA, USA). After allowing the cells to equilibrate overnight in the desired pH, 30 μL of 100 nM V7–750 or K7–750 probe was added to each well and the plates were then placed on a rocker mixer inside an incubator for 2 h. After incubation, all cells were washed 5 times with the corresponding pH-specific phosphate buffer (25 mM) to remove any unbound pHLIP probe. Fluorescent imaging and dosimetry was then performed using the Odyssey Infrared Imaging System (Li-COR, Lincoln, Nebraska, USA).

4) Human pancreatic cancer xenograft mouse models

Female athymic mice 4 weeks of age were used for this study in strict adherence to a University of Louisville Institutional Animal Care and Use Committee (IACUC) approved protocol. A diet of 2920× alfalfa-free feed (Harlan Laboratories, Indianapolis, USA) was used in order to reduce background signal during MSOT imaging. An established model for orthotopic implantation of pancreatic tumors was used as previously described. (26, 27) Briefly, mice were anesthetized with isoflurane and the abdomen was then prepped with betadine. A small incision was made in the left upper quadrant, with the pancreas exposed by retraction of the spleen. Luciferase-cloned S2VP10L and S2013Q cells were suspended in serum-free RPMI medium at 4°C in a sterile tube. After the pancreas was exposed, a solution of S2013Q 2.0×10^5 cells/30μL or S2VP10L 1.0×10^5 cells/30μL was injected into the pancreatic tail using a 28-gauge needle. To prevent peritoneal leakage, a sterile cotton tipped applicator was held over the injection site for 30 seconds. The organs were returned to the abdomen with the skin and peritoneum closed in a single layer using 5-0 prolene sutures. Mice recovered underneath a warming blanket and were returned to their cages with food and water *ad libitum* after regaining full mobility.

5) Tumor monitoring with bioluminescence imaging

Bioluminescence imaging was used immediately following surgery to assess potential leakage of cells from orthotopic implantation with the advanced molecular imager-1000-X (AMI) instrument (Spectral Imaging Instruments, Tucson, AZ, USA). Mice received i.p. injection of 2.5 mg luciferin 10 min prior to imaging, and those with signs of peritoneal leakage were excluded from further study. Sutures were removed after 5 days to prevent artifact during subsequent imaging studies. Tumor size was followed daily, and assessed again with bioluminescent imaging at 7 days post-op and prior to injection of the pHLIP probes. A similar procedure was utilized in previous work to identify the relative tumor location and size. (9,10) Based upon bioluminescence signal from orthotopic implants, 12 mice per S2VP10L and S2013Q cell line were selected to evaluate V7–750 and K7–750 probes. *In vivo*, 6 mice per probe were evaluated using MSOT. Each mouse was evaluated using planar fluorescence imaging at 0 and 4 h post probe injection immediately prior to MSOT imaging. *Ex vivo* organs from 3 mice per cell line per probe 4 h post injection (as indicated below) were evaluated via planar fluorescence imaging. *Ex vivo* tumor size was measured using calipers. The remaining 3 mice per cell line per probe were imaged a second time at 24 h with MSOT.

6) Evaluation of probe binding with Multispectral Optoacoustic Tomography

Immediately prior to injection as well as 4 and 24 h post injection, mice were imaged using an in Vision 256TF MSOT (iThera Medical, Munich, Germany). Mice placed ventral side up within the animal holder and positioned in a nose cone for anesthesia delivery. Anesthesia was maintained with 1.5% isoflurane in 0.8L medical air and 0.1L O_2 throughout image acquisition. Imaging was performed using axial slices with a 0.3-mm step through the liver-tumor-kidney region, at wavelengths of 680, 710, 730, 740, 750, 760,770, 780, 800, 850, 900 nm for each position. Ten wavelengths were selected based upon the spectra (Supplement Figure S1B) to allow for multispectral unmixing. Although individual frames

are not affected by animal motion, as the acquisition time per frame is less than one millisecond, 25 frames at each wavelength were obtained and averaged to compensate for animal motion and breathing artifacts (5). Respiration rate and signs of distress were monitored through all stages of the imaging procedure. After the last imaging time point of 24h, animals were euthanized via carbon dioxide overdose and cervical dislocation.

7) Image reconstruction and analysis

Raw data obtained with MSOT was reconstructed with multispectral analysis performed as previously described. (5, 6) Spectral analysis was performed at wavelengths corresponding to the Hilyte Fluor 750 dye. Spectra utilized for spectral unmixing are located within Supplement Figure 1B. Reconstruction was conducted using back projection at a resolution of 75 μm using View MSOT software version 3.5 (iThera Medical, Munich, Germany). The Multispectral Processing was conducted using Linear Regression with View MSOT 3.5, where known molar absorptivity spectra (e.g. for oxyhemoglobin, deoxyhemoglobin, and HiLyte Fluor 750) are used to model the relationship between chromophore concentration and MSOT signal over a range of wavelengths. The approach assumes knowledge about all absorbers present in the imaged tissue in order to correctly attribute contributions from the different wavelengths to the unmixed component images. (28) In order to ensure comparability among data sets, the reconstruction parameters (field of view, speed of sound, pixel size, and the high/low pass filters) and spectral unmixing parameters were consistently applied to all data. Spectral unmixing was performed in the absence of correction for fluence heterogeneities and attenuation as a function of tissue depth including spectral coloring. The authors note that the orthotopic tumors had a similar location and distance from the skin surface from animal to animal, thus fluence issues would equally affect all animals. Image stacks were imported into Image J for further evaluation of the 3D characteristics of probe binding within the tumor using orthogonal views. The location of orthotopic tumors was identified based upon the presence of deoxy-hemoglobin and relative location of the spleen and kidney (Supplemental Figure S2). In addition, a region of interest (ROI) method was applied to determine signal strength in the tumors of both K7–750 and V7–750 mice using View MSOT software and reported as MSOT a.u. The ROI was manually created with an ellipse drawing tool using the deoxyhemoglobin spectrally unmixed component as a guide for tumor location on the cross-section showing the largest area for the tumor (Supplement Figure S3). As in previous work, deoxyhemoglobin was utilized as a marker of tumor localization (29–31). The deoxyhemoglobin component was used to provide a basis for tumor segmentation in control (K7–750) animals, as there was significant overlap in signal localization between V7–750 and deoxyhemoglobin. The ROI area was kept constant for all image slices 3.5 mm^2, thus creating a non-uniform elliptical prism volume of interest (VOI). The mean pixel intensity per cross-section in the VOI for the spectrally unmixed injected agent (V7–750 or K7–750) was plotted as MSOT signal vs. position to assess the signal strength in the tumor. This analysis produced a consistent parabolic shape of signal over distance in the tumor. The maximal ‘mean signal per cross-section’ in the volume was used as a quantitative indicator of probe binding in the tumor. Since optoacoustic signals using the detection geometry of this system are subject to out-of-plane contributions, this method was used to find the center of signal intensity and minimize variability from out-of-plane artifacts. The capacity of this optoacoustic system to deliver semi-quantitative data reflective

of relative probe accumulation in vivo in murine models using the aforementioned reconstruction and multispectral unmixing methods was previously established. (30–36)The MSOT a.u. values for the pH-sensitive (V7–750) and pH-insensitive (K7–750) probes were compared using SAS 9.3 (Cary, NC).

8) Evaluation of probe binding with planar fluorescent imaging

Using a tail vein injection technique, 150 μL of the 40 μM V7–750 or of the K7–750 probe in sterile phosphate buffer (25 mM, 0.5 % NaCl, pH 7.4) was administered intravenously. Systemic injection of V7–750 or K7–750 was confirmed with near-infrared fluorescent imaging by AMI fluorescent imaging. NIR-fluorescence imaging was repeated prior to MSOT imaging at 4 and 24 h post-injection. Additionally, 3 mice per cell line were injected with V7–750 or K7–750 probes and organs (liver, kidney, and pancreas tumor) were removed 4 h post injection. Tissues were immediately placed into a petri dish with PBS 7.4 pH at 37°C, and within 30s from organ removal were imaged using NIR-fluorescence imaging (AMI).

9) Statistics

In vitro, comparison of signal intensity across pH levels for each cell line was performed with ANOVA using SAS 9.3 (SAS, Cary, NC). *In vivo*, the MSOT a.u. values for the pH-sensitive (V7–750) and pH-insensitive (K7–750) probes were compared using Wilcoxon sum-rank test and ANOVA followed by Tukey post hoc test using SAS 9.3 (Cary, NC). Significance was observed where $p < 0.05$.

Results

In vitro binding of pH sensitive or insensitive peptides

In vitro binding of the V7–750 or K7–750 probes was tested on both the S2VP10 and S2013 pancreatic cancer cell lines at pH 7.4, 6.8, and 6.6. In both S2VP10 and S2013 cells, V7–750 had significantly increased levels of fluorescence at pH_e 6.6 compared with pH_e 7.4 (S2VP10: 183.6 vs 9.1, p=0.0119; and S2013: 191.5 vs 10.2, p=0.0160). Furthermore, the signal intensity for V7–750 probe showed a consistently increasing trend across decreasing levels of pH_e in both cells lines (Figure 2). In contrast, the K7–750 displayed an insensitivity to acidic conditions, and had similarly low levels of fluorescence across all pH levels. In particular, no difference was observed between pH_e 7.4 and 6.6 in either cell line (S2VP10: 42.1 vs 44.3 MSOT a.u., p=0.8783; and S2013: 55.9 vs 38.7 MSOT a.u., p=0.7912).

MSOT imaging of pHLIP probes

MSOT imaging was performed on all mice at 4 and 24 hours post-injection. Localization of the V7–750 probes to the pancreatic bed was confirmed in the S2VP10 model, but no signal was detected with the K7–750 control probes (Figure 3). Quantification of multispectrally unmixed probe signal across the pancreas demonstrated a markedly higher mean value of MSOT a.u. for the V7–750 compared to K7–750 probe (S2VP10: 782.5 vs 5.3 MSOT a.u., p = 0.0001). In the S2013 model, V7–750 probe also specifically accumulated within the pancreas tumor in comparison to K7–750 control (S2013: 578.3 vs 5.1 MSOT a.u., p= 0.0005) (Supplemental Figure S4). The MSOT orthogonal views of the probe signal gave a

three-dimensional representation of the tumor bed, as well as its relationship to the surrounding internal anatomy. A further example of concordance of deoxy-hemoglobin within the S2VP10 pancreas tumor and V7–750 probe location is observed within a movie clip (Supplement Figure S5). Minimal off-target effects were observed with the pH-sensitive probes. In mice injected with the V7–750 probe, region of interest analysis demonstrated lower optoacoustic signal within the kidney and liver compared to the pancreatic bed. In contrast, the K7–750 control was noted to accumulate primarily within the kidney, with minimal signal observed in the area of the pancreas (Figure 4). Additionally, the V7–750 probe appears to distribute throughout the tumor bed in both models, with the highest signal intensity observed centrally within the tumor (Figure 5).

Planar fluorescent imaging of pHLIP probes

One week after tumor implantation, the mice had palpable lesions approximately 5 mm is size, with no signs of diffuse metastatic disease on bioluminescent imaging. Following injection of V7–750 on day 7, localization of fluorescent signal was observed in the right upper quadrant overlying the pancreas at the 4 hour time-point. Signal accumulation was not observed in the K7–750 controls (Figure 6A). By 24 hours, the probe signal was below AMI-detection in all mice. *Ex vivo* confirmation of probe location demonstrated significant accumulation of V7–750 within the pancreas compared to off-target organs in both the S2VP10 ($p=0.0002$) and S2013 ($p=0.0009$) models (Figure 6B). Non-specific accumulation of K7–750 in the kidney and liver was also observed (Figure 6B and Supplemental Figure S6).

Discussion

To the best of our knowledge, this is first study that uses optoacoustic tomography to characterize the internal distribution of acidic pH_e targeted probes *in vivo*. Our approach combining a pH targeted probe with MSOT imaging demonstrated substantial tumor-specific uptake of the pH-sensitive V7–750 probe, with minimal off-target accumulation. Conversely, the pH-insensitive probe demonstrated little to no focal accumulation within the pancreatic tumors.

While non-targeted contrast agents will partially accumulate in tumors through the enhanced permeable and retention effect (EPR), many contrast agents and nanotherapies employ a receptor-mediated targeting approach to enhance tumor-specificity and to improve internalization of molecular probes and drugs. (13, 37) However, molecular targeting strategies utilizing contrast agents with traditional imaging modalities typically have several drawbacks including limited tumor penetration, a susceptibility to degradation by the reticuloendothelial system, decreased circulation time, non-specific binding, increased clearance, or immunogenicity. (38–40) Targeted probes also may have off-target effects due to the inherent expression of the receptors in non-cancerous tissue.

Recently, alternatives to receptor or enzyme-mediated tumor targeting have focused on other tumor hallmarks such as acidosis and hypoxia in order to improve targeting and increase the signal-to-background ratio of contrast agents. (14, 15) Targeting and imaging of tumor acidity is an attractive strategy, as acidity typically is a general property of the tumor

microenvironment. Acidosis results during tumor development at both early and advanced stages from a combination of factors such as hypoxia, anaerobic glycolysis (Warburg effect) and carbonic anhydrase activity. (16) In fact, *in vitro* studies suggest that tumor proliferation is maximized by acidic pH, and there is a measurable difference in the extracellular pH of solid tumors (pH 6.5–6.9) when compared to normal tissue (pH 7.2–7.4). (41–45) Targeting the acidic microenvironment also avoids the complication of tumor resistance and natural selection issues that contribute to an evolving tumor phenotype, including alterations in extra-cellular receptor expression.

In this study, the acidic environment of pancreatic tumors was targeted by using a pH low insertion peptide (pHLIP). These peptides consist of a transmembrane domain with two flanking domains, and exist in three pH-dependent states: I) as a monomer in solution II) as a monomer bound at the surface of the lipid bilayer or III) as a transmembrane α-helix. (21) Protonation of glutamate residues at acidic pH leads to a conformational change of the transmembrane domain to a stable α-helix, which inserts into cellular membranes (Figure 1). The insertion of pHLIPs in lipid bilayers is a spontaneous process and is accompanied by energy release. After insertion, the *N*-terminus remains in the extracellular space and the C-terminus enters the intracellular lumen, giving these peptides the dual capability of tethering molecules such as fluorophores attached to the N-terminus on the extra-cellular membrane, while carrying molecules attached to the C-terminus into the cytosol. (15) Several prior studies have demonstrated that pHLIPs are promising candidates for targeted therapy, and can localize to a variety of tumors *in vivo*. (46–47)

Recently, Cruz-Monserrate et al. demonstrated that fluorescent-tagged pHLIPs localize to human pancreatic cancer xenografts in mice. (48) However, in their study the pancreatic tumors were imaged using 2D planar fluorescent imaging at only a 24 h time point, and a pH-insensitive pHLIP was not used as a control for the orthotopic model. We build upon these results in our study, but we utilize an emerging imaging technology that has feasible clinical translation and we ensure acidic pH_e tumor targeting by using a pH-insensitive control. As suggested by both our *in vitro* and *in vivo* results, the K7–750 peptide does not insert into the lipid bilayer of tumor cells at physiologic or acidic pH_e. On the other hand, the pH-sensitive V7–750 probe localized to orthotopic PDACs at 4 h as observed by MSOT (Figures 3–5, Supplemental Figures S4–S5). In the S2VP10 cells, MSOT detected statistically significant accumulation of the V7–750 probe, 782.5 MSOT a.u., compared to that of the K7–750 probe, 5.3 MSOT a.u. ($p=0.0001$); the V7–750 probe accumulation 578.3 MSOT a.u. compared to that of the K7–750 probe, 5.1 MSOT a.u., in the tumors in the S2013 mice ($p=0.0005$). Furthermore, the MSOT orthogonal views demonstrated good penetration of the V7–750 probe throughout the tumor bed, with very limited accumulation outside of the tumor.

MSOT exhibits several advantages over other imaging techniques; traditional bio-imaging modalities require ionizing radiation and may lack the combination of high resolution and depth of penetration provided by MSOT. (49–52) In contrast, MSOT provides contrasted images at a microscale (μm) resolution, and provides a reasonable penetration depth by combining the advantages of optical imaging (high sensitivity) and ultrasonic detection (increased depth of penetration). (5) MSOT renders photon scattering irrelevant to image

formation, and the addition of molecularly targeted optical contrast enables the capability for novel high-resolution insights into the biological function of entire tumors, organs, and systems. (9) As such, MSOT combines anatomical and molecular information in a single, high-resolution modality.

The use of exogenous contrast agents with a large optical absorption is an additional advantage of MSOT imaging, as exogenous contrast agents can produce MSOT signal several-fold higher in magnitude than signal originating from native tissue. (53) Exogenous contrast agents can also improve imaging by using infra-red dye (650–1100 nm) at a spectrum where endogenous tissue components have minimal absorption. Additionally, due to the sensitivity of MSOT, only a low volume of optical contrast is required, which can be an advantage when imaging tumor acidity. While acidosis is an attractive target for tumor imaging, the pKa of the contrast agent must match acidic extracellular tumor pH, or detection of the optical reporter *in vivo* can be troublesome. Since the required concentration of the contrast agent can buffer the tumor microenvironment and subsequently alter the tissue pH_e, successful detection of tumors using pH-sensitive probes becomes difficult. (54–55) Optical-based contrast agents generally require low concentration, thus the risk of contrast agent buffering the tissue pH_e is low.

Clinical translation of optoacoustic imaging strategies in preclinical models is currently under way; however, its use presents certain challenges. One of the principle limitations is depth of imaging; increasing the depth requires lower ultrasound frequencies that are more subject to signal attenuation. (56) Nonetheless, existing photoacoustic systems have been shown to achieve adequate spatial resolution with tissue penetration up to 6–7 cm in some clinical and experimental studies. (57–58) While at this time the limited penetration depth precludes the use of MSOT for total body imaging in a manner akin to CT or MRI, current photoacoustic imaging technologies could serve as an adjunct to invasive staging or therapeutic procedures such as laparoscopy, endoscopy, or intraoperative ultrasonography. (56) However, further improvement of the technology and development of targeted, exogenous contrast agents may allow for deeper imaging. (24) Additionally, the molecular imaging capability of MSOT can provide functional information that is not attainable with CT or MRI.

Current clinical versions of MSOT may be used to image ductal pancreatic adenocarcinomas (PDACs) that are within 5 cm of the MSOT transducer. At this depth, MSOT images provide not only a clear image of the tumors and associated vessels via detecting hemoglobin, but also specific molecular information concerning the PDACs. PDACs frequently are evaluated by ultrasound to distinguish the involvement of major arteries and/or veins by the tumor and thus stratifying patients by stage for potential surgical intervention and indicating which borderline patients are candidates for resection. Because the majority of patients are diagnosed with advanced PDAC, neoadjuvant therapy can sometimes be used to reduce tumor burden and permit radical pancreatic surgery (59–60); however, the resulting fibrous tissue and scar frequently remain indistinguishable from viable tumor using traditional endoscopic ultrasound. The use of endoscopic and/or laparoscopic clinical MSOT imaging with cellular molecular probes, such as V7–750, should permit the separation of viable tumor from fibrous tissue and scar. Clinical MSOT

should be especially useful for imaging pancreatic cancer by monitoring the effectiveness of neoadjuvant therapy and stratification of PCDAs for surgical intervention, permitting tumor removal by pancreatectomy.

In addition, although acquisition time could be seen as a limitation, reconfiguration of the MSOT settings allows for faster imaging times. For instance, achieving molecular specificity entails a spectral unmixing process that operates on a pixel-by-pixel basis which can be compromised by motion artifacts. In the current study, averaging data from multiple sequential laser pulses was used as a facile motion correction strategy. Considering the averaging (25 pulses at 10Hz) and the number of wavelengths (n=10) used for imaging, the temporal resolution per cross-section was 25 seconds. Although it was not the focus of this study, optimization of the acquired wavelengths and averaging, in combination with the use of a laser with a 50Hz repetition rate, can produce faster multispectral results up to 2Hz for handheld imaging in human subjects, enabling imaging on a faster time scale than observer or patient motion. (61) While these preliminary studies using a hand-held MSOT indicate potential clinical use, we believe that the addition of targeted contrast agents, such as V7–750, could allow for identification of pancreatic tumors in the clinical setting with similarities to diagnostic sonography, endoscopy and laparoscopy.

In the future, we expect that the combination of acidic pH_e contrast agents and use of MSOT will result in more sensitive and specific detection of tumors in real-time, improving the imaging of pancreatic cancer. Beyond improved imaging of pancreatic cancer, we anticipate the use of pH_e responsive contrast agents in combination with MSOT to be broadly applicable to other solid tumors, since acidic pH_e is a general feature of the tumor microenvironment. Acidic pH_e-responsive contrast agents could facilitate image-guided surgical removal of both the primary cancer and metastasis. Additionally, acidic pH_e imaging could stratify patients for pH-specific drug delivery. Translation of MSOT technology to the clinic through handheld or endoscopic arrays is currently under development. (25, 62) It is hoped that the advances proposed will improve patient outcomes for these poorly detectable cancers.

Conclusion

We constructed pH-sensitive (V7–750) and pH-insensitive (K7–750) fluorescent probes in order to target the acidic tumor microenvironment and detect pancreatic cancer cells *in vivo* via MSOT. Targeting the acidic extracellular pH of tumor cells helps resolve problems associated with receptor-mediated targeting; acidosis is a major characteristic of the tumor environment, and is not as naturally heterogeneous as extracellular receptors or proteins. Utilization of MSOT enabled detection of pancreatic tumors at 4 h after intravenous injection of pH-sensitive probes, while the pH-insensitive probes did not localize to the pancreatic tumors. Furthermore, *in vivo* imaging demonstrated that V7–750 preferentially accumulated in the tumor bed with minimal off-target effects. Acidic pH-responsive peptides have potential use for both clinical cancer diagnostics and drug delivery, and MSOT is a promising modality for non-invasive detection and quantification of these probes *in vivo*. As MSOT equipment is now available for human clinical research and as the

technology continues to improve, the translation of these techniques to clinical cancer detection and monitoring warrants further evaluation and development.

Supplementary Material

Refer to Web version on PubMed Central for supplementary material.

Acknowledgements

This work was funded in part by the Rounsavall Foundation and the UAB/UMN SPORE in Pancreatic Cancer: Tissue Resources and Molecular Pathology Core 2P50CA101955.

Sources

1. Cancer Facts and Figures 2014. Atlanta: American Cancer Society; 2014.
2. Kaur S, Baine MJ, Jain M, Sasson AR, Batra SK. Early diagnosis of pancreatic cancer: challenges and new developments. Biomarkers in medicine. 2012; 6(5):597–612. [PubMed: 23075238]
3. Orbay H, Bean J, Zhang Y, Cai W. Intraoperative targeted optical imaging: a guide towards tumor-free margins in cancer surgery. Current pharmaceutical biotechnology. 2013; 14(8):733–742. [PubMed: 24372232]
4. Ntziachristos V. Going deeper than microscopy: the optical imaging frontier in biology. Nature methods. 2010; 7(8):603–614. [PubMed: 20676081]
5. Razansky D, Buehler A, Ntziachristos V. Volumetric real-time multispectral optoacoustic tomography of biomarkers. Nature protocols. 2011; 6(8):1121–1129. [PubMed: 21738125]
6. Buehler A, Herzog E, Ale A, Smith BD, Ntziachristos V, Razansky D. High resolution tumor targeting in living mice by means of multispectral optoacoustic tomography. EJNMMI research. 2012; 2:14. [PubMed: 22464315]
7. Ntziachristos V, Bremer C, Weissleder R. Fluorescence imaging with near-infrared light: new technological advances that enable in vivo molecular imaging. European radiology. 2003; 13(1): 195–208. [PubMed: 12541130]
8. Marelli UK, Rechenmacher F, Sobahi TR, Mas-Moruno C, Kessler H. Tumor Targeting via Integrin Ligands. Frontiers in oncology. 2013; 3:222. [PubMed: 24010121]
9. Hudson SV, Huang JS, Yin W, Albeituni S, Rush J, Khanal A, et al. Targeted Noninvasive Imaging of EGFR-Expressing Orthotopic Pancreatic Cancer Using Multispectral Optoacoustic Tomography. Cancer research. 2014; 74(21):6271–6279. [PubMed: 25217521]
10. Kimbrough CW, Hudson S, Khanal A, Egger ME, McNally LR. Orthotopic pancreatic tumors detected by optoacoustic tomography using Syndecan-1. The Journal of surgical research. 2014
11. Catenacci DV. Next-generation clinical trials: Novel strategies to address the challenge of tumor molecular heterogeneity. Molecular oncology. 2014
12. Du W, Elemento O. Cancer systems biology: embracing complexity to develop better anticancer therapeutic strategies. Oncogene. 2014
13. Karra N, Benita S. The ligand nanoparticle conjugation approach for targeted cancer therapy. Current drug metabolism. 2012; 13(1):22–41. [PubMed: 21892918]
14. Andreev OA, Engelman DM, Reshetnyak YK. Targeting diseased tissues by pHLIP insertion at low cell surface pH. Frontiers in physiology. 2014; 5:97. [PubMed: 24659971]
15. Deacon JC, Engelman DM, Barrera FN. Targeting acidity in diseased tissues: Mechanism and applications of the membrane-inserting peptide, pHLIP. Archives of biochemistry and biophysics. 2014; 565c:40–48. [PubMed: 25444855]
16. Gillies RJ, Verduzco D, Gatenby RA. Evolutionary dynamics of carcinogenesis and why targeted therapy does not work. Nature reviews Cancer. 2012; 12(7):487–493.
17. Fang JS, Gillies RD, Gatenby RA. Adaptation to hypoxia and acidosis in carcinogenesis and tumor progression. Seminars in cancer biology. 2008; 18(5):330–337. [PubMed: 18455429]

18. Wojtkowiak JW, Rothberg JM, Kumar V, Schramm KJ, Haller E, Proemsey JB, et al. Chronic autophagy is a cellular adaptation to tumor acidic pH microenvironments. Cancer research. 2012; 72(16):3938–3947. [PubMed: 22719070]

19. Bellocq A, Suberville S, Philippe C, Bertrand F, Perez J, Fouqueray B, et al. Low environmental pH is responsible for the induction of nitric-oxide synthase in macrophages. Evidence for involvement of nuclear factor-kappaB activation. The Journal of biological chemistry. 1998; 273(9):5086–5092. [PubMed: 9478960]

20. Kong SC, Gianuzzo A, Novak I, Pedersen SF. Acid-base transport in pancreatic cancer: molecular mechanisms and clinical potential. Biochemistry and cell biology = Biochimie et biologie cellulaire. 2014; 92(6):449–459. [PubMed: 25372771]

21. Weerakkody D, Moshnikova A, Thakur MS, Moshnikova V, Daniels J, Engelman DM, et al. Family of pH (low) insertion peptides for tumor targeting. Proceedings of the National Academy of Sciences of the United States of America. 2013; 110(15):5834–5839. [PubMed: 23530249]

22. Reshetnyak YK, Andreev OA, Segala M, Markin VS, Engelman DM. Energetics of peptide (pHLIP) binding to and folding across a lipid bilayer membrane. Proceedings of the National Academy of Sciences of the United States of America. 2008; 105(40):15340–15345. [PubMed: 18829441]

23. Buehler A, Kacprowicz M, Taruttis A, Ntziachristos V. Real-time handheld multispectral optoacoustic imaging. Optics letters. 2013; 38(9):1404–1406. [PubMed: 23632499]

24. Dean-Ben XL, Razansky D. Functional optoacoustic human angiography with handheld video rate three dimensional scanner. Photoacoustics. 2013; 1(3–4):68–73. [PubMed: 25302151]

25. Deán-Ben XL, Razansky D. Portable spherical array probe for volumetric real-time optoacoustic imaging at centimeter-scale depths. Optics express. 2013; 21(23):28062–28071. [PubMed: 24514320]

26. McNally LR, Welch DR, Beck BH, Stafford LJ, Long JW, Sellers JC, et al. KISS1 over-expression suppresses metastasis of pancreatic adenocarcinoma in a xenograft mouse model. Clinical & experimental metastasis. 2010; 27(8):591–600. [PubMed: 20844932]

27. DeRosier LC, Buchsbaum DJ, Oliver PG, Huang ZQ, Sellers JC, Grizzle WE, et al. Combination treatment with TRA-8 anti death receptor 5 antibody and CPT-11 induces tumor regression in an orthotopic model of pancreatic cancer. Clinical cancer research : an official journal of the American Association for Cancer Research. 2007; 13(18 Pt 2):5535s–5543s. [PubMed: 17875786]

28. Tzoumas S, Deliolanis N, Morscher S, Ntziachristos V. Un-mixing Molecular Agents from Absorbing Tissue in Multispectral Optoacoustic Tomography. IEEE transactions on medical imaging. 2013

29. Liu J, Zheng X, Yan L, Zhou L, Tian G, Yin W, Wang L, Liu Y, Hu Z, Gu Z, Chen C, Zhao Y. Bismuth sulfide nanorods as a precision nanomedicine for in vivo multimodal imaging-guided photothermal therapy of tumor. ACS Nano. 2015; 9(1):696–707. [PubMed: 25561009]

30. Beziere N, Lozano N, Nunes A, Salichs J, Queiros D, Kostarelos K, Ntziachristos V. Dynamic imaging of PEGylated indocyanine green (ICG) liposomes within the tumor microenvironment using multi-spectral optoacoustic tomography (MSOT). Biomaterials. 2015; 37:415–424. [PubMed: 25453969]

31. Burton NC, Patel M, Morscher S, Driessen WH, Claussen J, Beziere N, Jetzfellner T, Taruttis A, Razansky D, Bednar B, Ntziachristos V. Multispectral opto-acoustic tomography (MSOT) of the brain and glioblastoma characterization. Neuroimage. 2013; 65:522–528. [PubMed: 23026761]

32. Wu W, Driessen W, Jiang X. Oligo(ethylene glycol)-based thermosensitive dendrimers and their tumor accumulation and penetration. J Am Chem Soc. 2014; 136(8):3145–3155. [PubMed: 24506735]

33. Dinish US, Song Z, Ho CJH, Balasundaram G, Attia ABE, Lu X, Tang BZ, Liu B, Olivo M. Single Molecule with Dual Function on Nanogold: Biofunctionalized Construct for In Vivo Photoacoustic Imaging and SERS Biosensing. Adv. Funct. Mater. 2015; 25:2316–2325.

34. Attia AB, Balasundaram G, Driessen W, Ntziachristos V, Olivo M. Phthalocyanine photosensitizers as contrast agents for in vivo photoacoustic tumor imaging. Biomed Opt Express. 2015; 6(2):591–598. [PubMed: 25780748]

35. Ye S, Marston G, McLaughlan JR, Sigle DO, Ingram N, Freear S, Evans SD. Engineering Gold Nanotubes with Controlled Length and Near-Infrared Absorption for. Adv. Funct. Mater. 2015; 25(14):2117–2127.
36. Morscher S, Driessen WH, Claussen J, Burton NC. Semi-quantitative Multispectral Optoacoustic Tomography (MSOT) for volumetric PK imaging of gastric emptying. Photoacoustics. 2014; 2(3): 103–110. [PubMed: 25431754]
37. Weissleder R, Pittet MJ. Imaging in the era of molecular oncology. Nature. 2008; 452(7187):580–589. [PubMed: 18385732]
38. Herzog E, Taruttis A, Beziere N, Lutich AA, Razansky D, Ntziachristos V. Optical imaging of cancer heterogeneity with multispectral optoacoustic tomography. Radiology. 2012; 263(2):461–468. [PubMed: 22517960]
39. Hellebust A, Richards-Kortum R. Advances in molecular imaging: targeted optical contrast agents for cancer diagnostics. Nanomedicine (London, England). 2012; 7(3):429–445.
40. Kelloff GJ, Krohn KA, Larson SM, Weissleder R, Mankoff DA, Hoffman JM, et al. The progress and promise of molecular imaging probes in oncologic drug development. Clinical cancer research : an official journal of the American Association for Cancer Research. 2005; 11(22): 7967–7985. [PubMed: 16299226]
41. Gillies RJ, Gatenby RA. Hypoxia and adaptive landscapes in the evolution of carcinogenesis. Cancer metastasis reviews. 2007; 26(2):311–317. [PubMed: 17404691]
42. Zhang X, Lin Y, Gillies RJ. Tumor pH and its measurement. Journal of nuclear medicine : official publication, Society of Nuclear Medicine. 2010; 51(8):1167–1170.
43. Estrella V, Chen T, Lloyd M, Wojtkowiak J, Cornnell HH, Ibrahim-Hashim A, et al. Acidity generated by the tumor microenvironment drives local invasion. Cancer research. 2013; 73(5): 1524–1535. [PubMed: 23288510]
44. Stubbs M, McSheehy PM, Griffiths JR, Bashford CL. Causes and consequences of tumour acidity and implications for treatment. Molecular medicine today. 2000; 6(1):15–19. [PubMed: 10637570]
45. Gillies RJ, Liu Z, Bhujwalla Z. 31P-MRS measurements of extracellular pH of tumors using 3-aminopropylphosphonate. The American journal of physiology. 1994; 267(1 Pt 1):C195–C203. [PubMed: 8048479]
46. Adochite RC, Moshnikova A, Carlin SD, Guerrieri RA, Andreev OA, Lewis JS, et al. Targeting breast tumors with pH (low) insertion peptides. Molecular pharmaceutics. 2014; 11(8):2896–2905. [PubMed: 25004202]
47. Reshetnyak YK, Yao L, Zheng S, Kuznetsov S, Engelman DM, Andreev OA. Measuring tumor aggressiveness and targeting metastatic lesions with fluorescent pHLIP. Molecular imaging and biology : MIB : the official publication of the Academy of Molecular Imaging. 2011; 13(6):1146–1156. [PubMed: 21181501]
48. Cruz-Monserrate Z, Roland CL, Deng D, Arumugam T, Moshnikova A, Andreev OA, et al. Targeting pancreatic ductal adenocarcinoma acidic microenvironment. Scientific reports. 2014; 4:4410. [PubMed: 24642931]
49. Ntziachristos V, Ripoll J, Wang LV, Weissleder R. Looking and listening to light: the evolution of whole-body photonic imaging. Nature biotechnology. 2005; 23(3):313–320.
50. Mallidi S, Luke GP, Emelianov S. Photoacoustic imaging in cancer detection, diagnosis, and treatment guidance. Trends in biotechnology. 2011; 29(5):213–221. [PubMed: 21324541]
51. Wang LV, Hu S. Photoacoustic tomography: in vivo imaging from organelles to organs. Science. 2012; 335(6075):1458–1462. [PubMed: 22442475]
52. Luker GD, Luker KE. Optical imaging: current applications and future directions. Journal of nuclear medicine : official publication, Society of Nuclear Medicine. 2008; 49(1):1–4.
53. Su JL, Wang B, Wilson KE, Bayer CL, Chen YS, Kim S, et al. Advances in Clinical and Biomedical Applications of Photoacoustic Imaging. Expert opinion on medical diagnostics. 2010; 4(6):497–510. [PubMed: 21344060]
54. Sheth VR, Liu G, Li Y, Pagel MD. Improved pH measurements with a single PARACEST MRI contrast agent. Contrast Media & Molecular Imaging. 2012; 7(1):26–34. [PubMed: 22344877]

55. Gallagher FA, Kettunen MI, Day SE, Hu D-E, Ardenkjaer-Larsen JH, Zandt Rit, et al. Magnetic resonance imaging of pH in vivo using hyperpolarized 13C-labelled bicarbonate. Nature. 2008; 453(7197):940–943. [PubMed: 18509335]

56. Zackrisson S, van de Ven SM, Gambhir SS. Light in and sound out: emerging translational strategies for photoacoustic imaging. Cancer research. 2014; 74(4):979–1004. [PubMed: 24514041]

57. Pramanik M, Ku G, Li C, Wang LV. Design and evaluation of a novel breast cancer detection system combining both thermoacoustic (TA) and photoacoustic (PA) tomography. Medical physics. 2008; 35(6):2218–2223. [PubMed: 18649451]

58. Manohar S, Vaartjes SE, van Hespen JC, Klaase JM, van den Engh FM, Steenbergen W, et al. Initial results of in vivo non-invasive cancer imaging in the human breast using near-infrared photoacoustics. Optics express. 2007; 15(19):12277–12285. [PubMed: 19547596]

59. Patel M, Hoffe S, Malafa M, Hodul P, Klapman J, Centeno B, Kim J, Helm J, Valone T, Springett G. Neoadjuvant GTX Chemotherapy and IMRT-Based Chemoradiation for Borderline Resectable Pancreatic Cancer. Journal of Surgical Oncology. 2011; 104(2):155–161. [PubMed: 21520097]

60. Katz MHG, Fleming JB, Bhosale P, Varadhachary G, Lee JE, Wolff R, Wang H, Abbruzzese J, Pisters PWT, Vauthey JN, Charnsangavej C, Tamm E, Crane CH, Balachandran A. Response of borderline resectable pancreatic cancer to neoadjuvant therapy is not reflected by radiographic indicators. Cancer. 2012; 118(23):5749–5756. [PubMed: 22605518]

61. Taruttis A, Rosenthal A, Kacprowicz M, Burton NC, Ntziachristos V. Multiscale multispectral optoacoustic tomography by a stationary wavelet transform prior to unmixing. IEEE transactions on medical imaging. 2014; 33(5):1194–1202. [PubMed: 24770922]

62. Yang JM, Favazza C, Chen R, Yao J, Cai X, Maslov K, et al. Simultaneous functional photoacoustic and ultrasonic endoscopy of internal organs in vivo. Nature medicine. 2012; 18(8): 1297–1302.

Translational Aspect

Pancreatic ductal adenocarcinoma (PDAC) remains highly lethal because of its advanced stage at presentation, which is partly due to the lack of effective approaches to identify tumors early. Molecular imaging with targeted probes could potentially improve the early diagnosis, staging, and monitoring of PDAC. Using an orthotopic xenograft model of PDAC, our results indicate that pH-sensitive probes will localize to pancreatic tumors, and combining these probes with multispectral optoacoustic tomography (MSOT) can precisely map probe location with 3-dimensional imaging. Endoscopic, laparoscopic, or handheld applications of MSOT in combination with pH-sensitive probes could aid in the detection and staging of pancreatic tumors, help determine resectability, assist in identification of viable tumor during surgical intervention, as well as help monitor responses to treatment. Further development of MSOT imaging technology using pH-sensitive probes may lead to improvements in tumor imaging, treatment, and follow-up for pancreatic cancer.

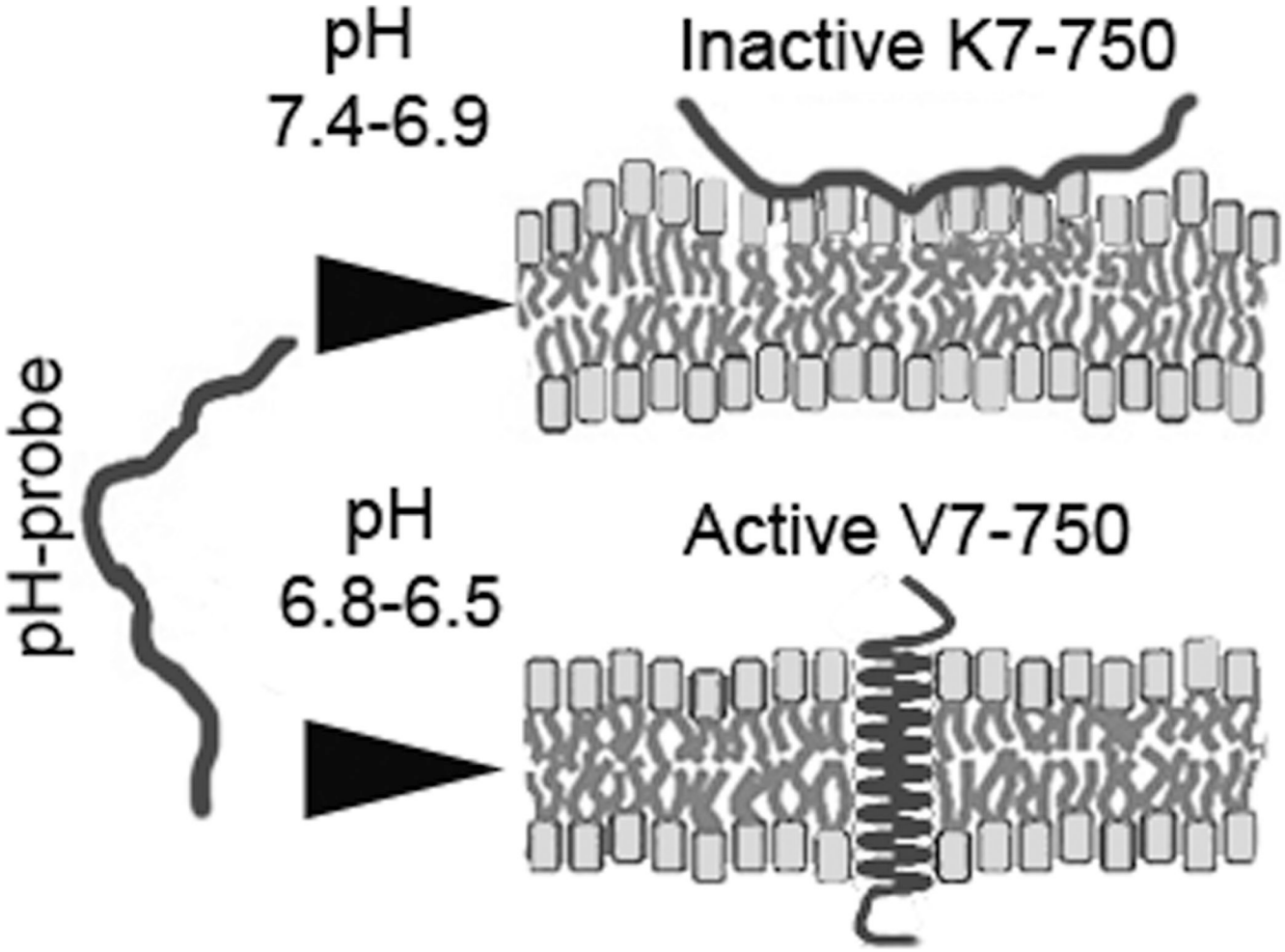

Figure 1.
Schematic of probe insertion into cell membrane.

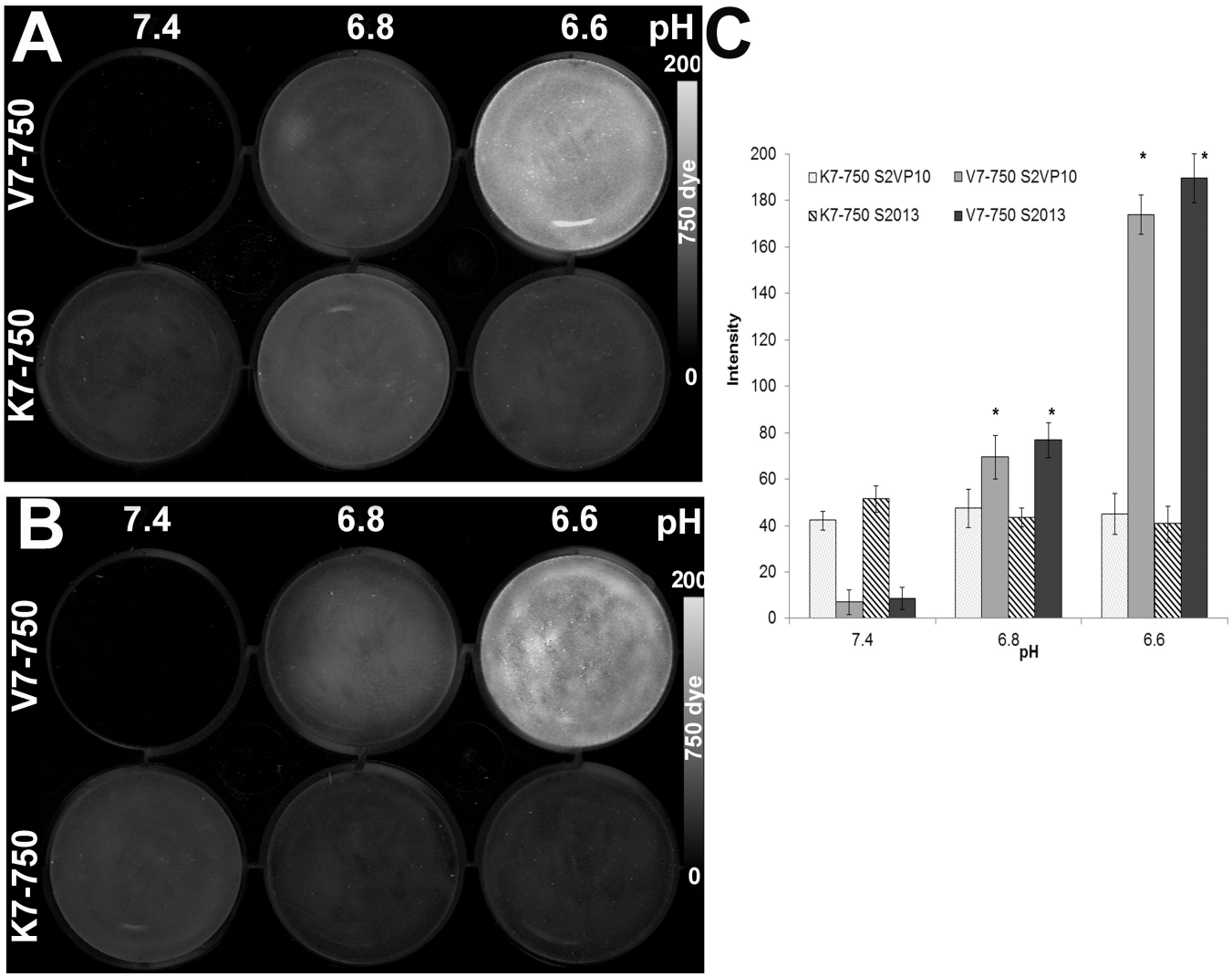

Figure 2.

In vitro testing of probe binding to pancreatic cancer cells at different levels of media acidity. (A) S2VP10 cells treated with either V7–750 (top row) or K7–750 (bottom row) at different levels of media pH. The experiment was repeated for S2013 cells (B). Dosimetry quantifies the signal intensity for each cell line at different pH values (C).

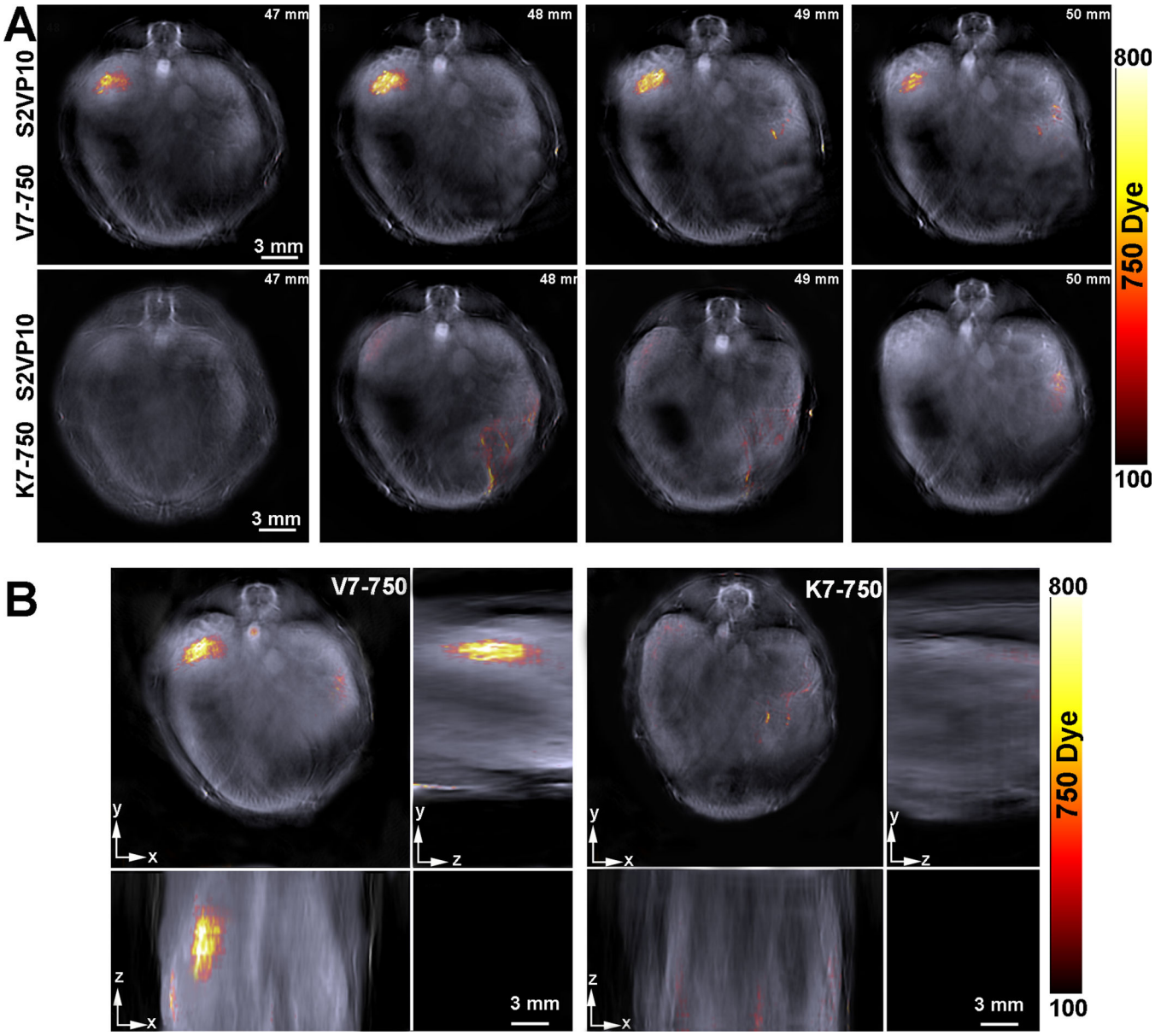

Figure 3.

Axial tomographic slices of the S2VP10 mouse demonstrate localization of V7–750 probe signal to the region of the tumor bed, while similar signal is not observed with K7–750 probe. The gray scale image represents a single wavelength, 850 nm, and serves as a background image. (A) Single slices from 47 mm– 50 mm of mice demonstrate distribution of V7–750 probe signal throughout the tumor bed at 4 hours, while minimal accumulation is observed with K7–750. (B) Orthogonal images demonstrate 3D accumulation of V7–750 and K7–750 within the mouse in the xyz-plane.

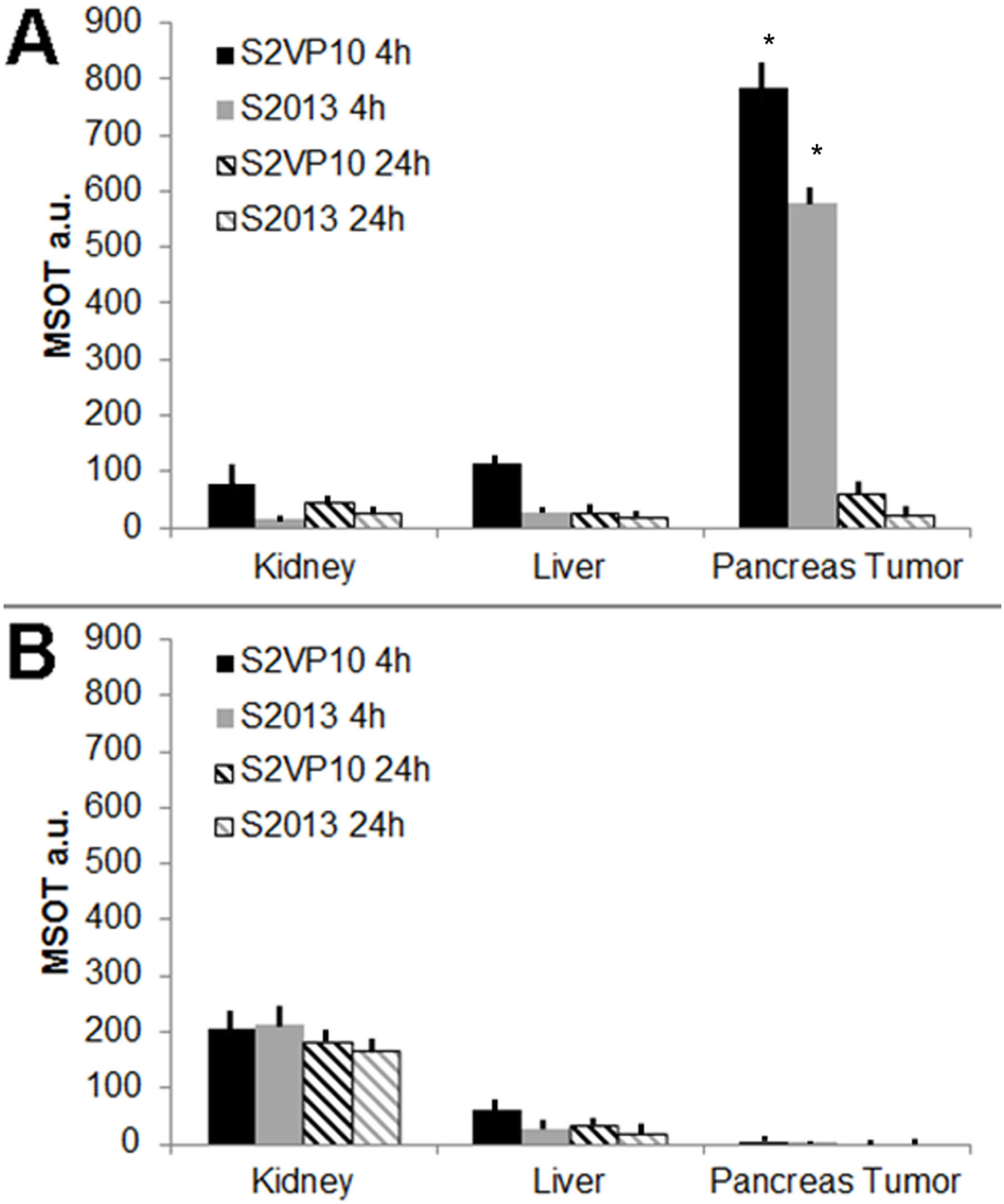

Figure 4.

Comparison of MSOT signal intensity of probe accumulation among organs. A region of interest method was utilized using an elliptical ROI of 3.5 mm^2 in a region of pancreas tumor, liver, and kidney was utilized to determine the mean signal intensity for each ROI in each slice. (A) The highest ROI mean signal intensity for each organ and each mouse was averaged among 3 mice per cell line injected with V7–750 probe. The V7–750 probe resulted in 782.5 MSOT a.u. in S2VP10 mice and 578.3 MSOT a.u. in S2O13 mice at 4 h, but was greatly reduced to 73.5 and 34.2 MSOT a.u. at 24 h. (B) The highest ROI mean

signal intensity for each organ and each mouse was averaged among 3 mice per cell line injected with K7–750 probe. The K7–750 probe accumulated within the kidney and only resulted in very limited pancreas tumor accumulation in either S2VP10 (5.3 MSOT a.u.) or S2013 (5.1 MSOT a.u.) models.

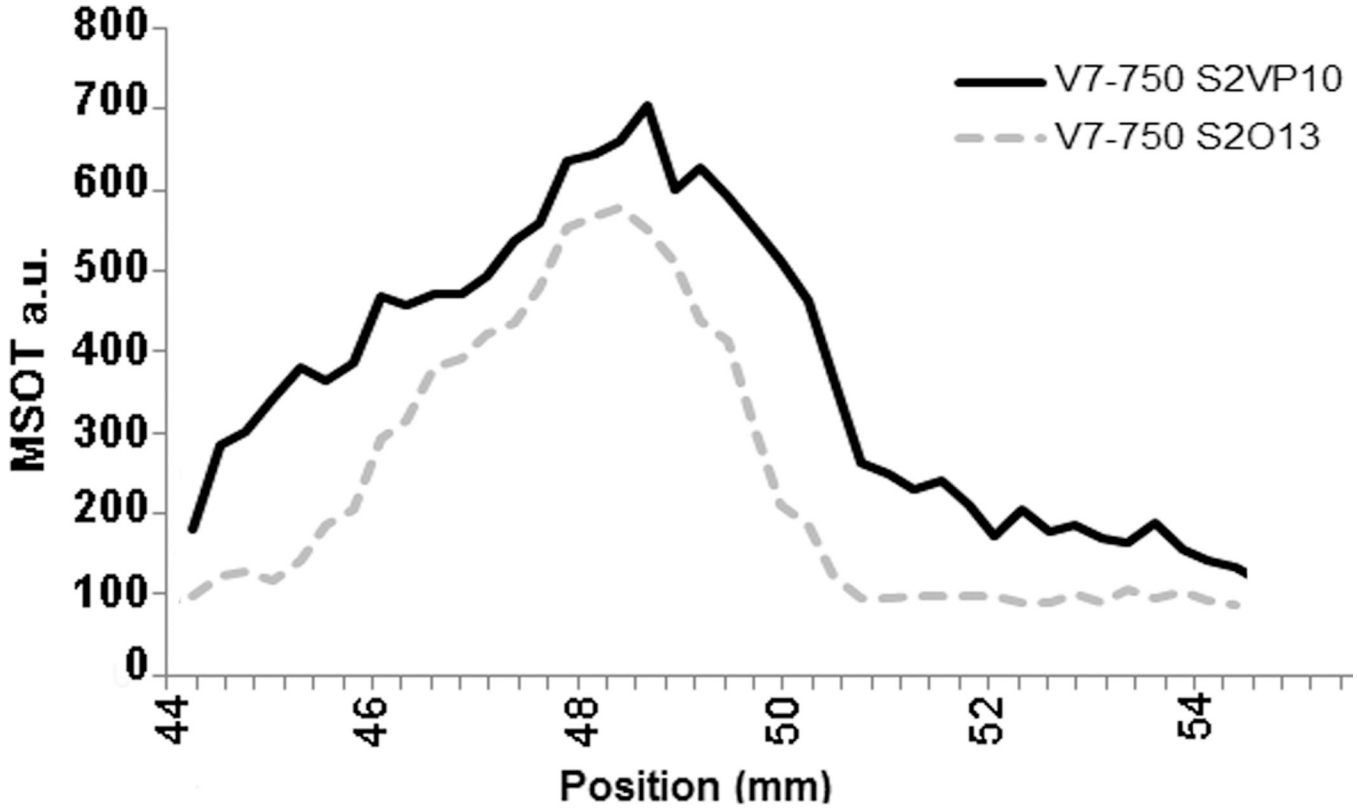

Figure 5.

Analysis of the regions of interest of the pancreas show V7–750 accumulated with a maximum peak at 49.2 mm in S2VP10 and 48.4 mm in S2O13 model. The area utilized for region of interest measurements remained constant for each slice. Image quantification for each organ is shown in Figure 4.

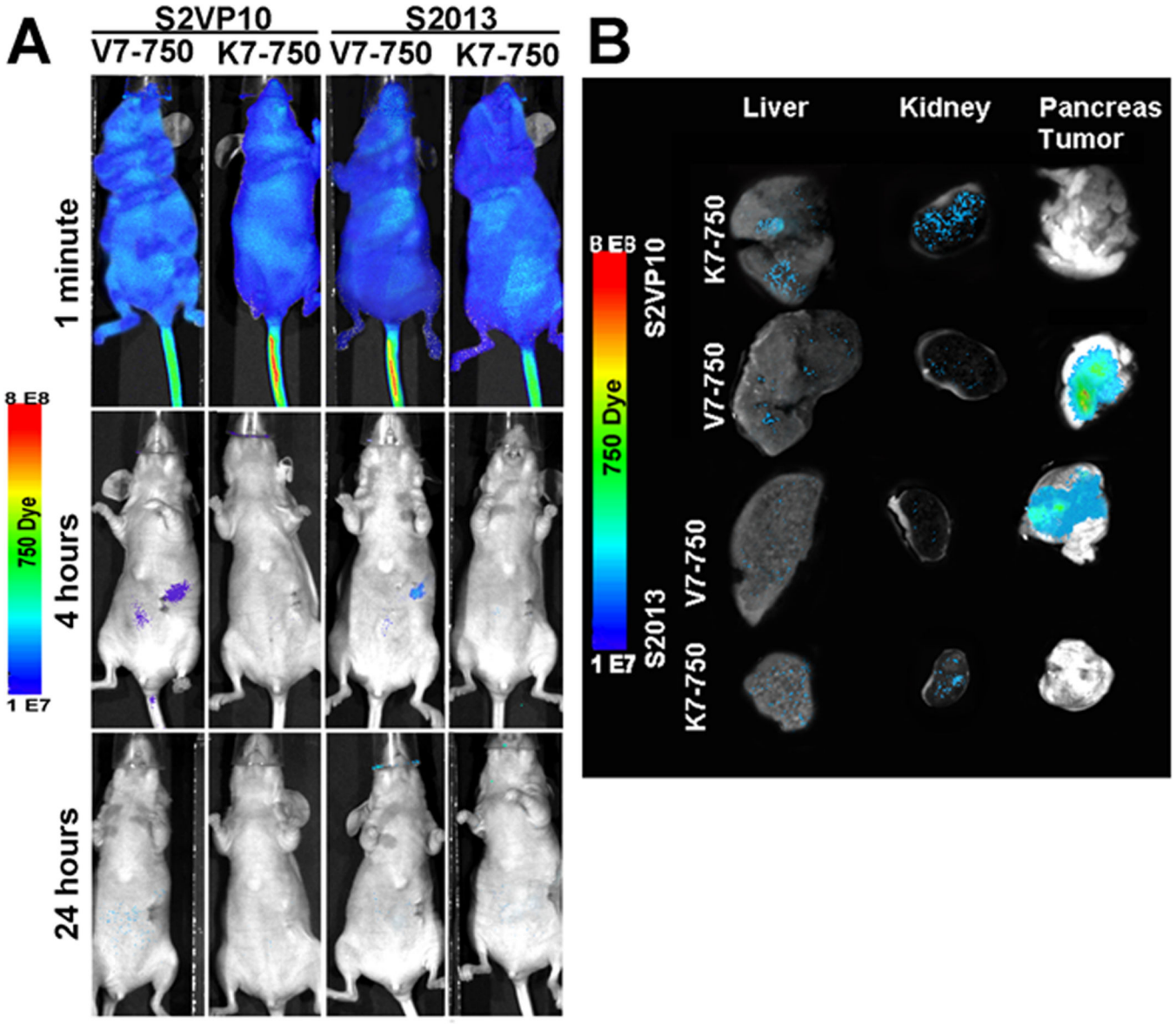

Figure 6.

Traditional planar fluorescent imaging of probe signal immediately following injection, at 4 hours post-injection, and at 24 hours post-injection. (A) Although both probes are distributed systemically with similar signal intensity, the V7–750 pHLIP localizes to the pancreas at the 4 hour time point with diminishing signal at 24h. (B) *Ex vivo* identification of V7–750 and K7–750 in liver, kidney, and pancreas tumor. Images were quantified in Supplemental Figure S6.